Chemical Engineering Journal 488 (2024) 151037

Contents lists available at ScienceDirect

Chemical Engineering Journal

journal homepage: www.elsevier.com/locate/cej

Tailoring anion exchange membranes for palladium recovery from industrial solutions using electrodialysis

Önder Tekinalp [a], Xueru Wang [a], Pauline Zimmermann [b], Odne Stokke Burheim [b], Liyuan Deng [a,*]

[a] Department of Chemical Engineering, Norwegian University of Science and Technology (NTNU), NO-7491 Trondheim, Norway
[b] Department of Energy and Process Engineering, Norwegian University of Science and Technology (NTNU), NO-7491 Trondheim, Norway

ARTICLE INFO

Keywords:
Anion exchange membrane
Electrodialysis
Palladium recovery
Quaternary ammonium

ABSTRACT

Limited natural reserves and extensive use of palladium across various industries make it urgent to implement efficient recovery strategies. Despite its unique advantages, the use of ion exchange membranes in electrodialysis to recover palladium species from diverse sources remains unexplored. This study focuses on tailoring anion exchange membranes (AEMs) for the recovery of palladium tetrachloride ($[PdCl_4]^{2-}$) from industrial hydrochloric acid-based solutions (pH below 1) in electrodialysis, aiming to overcome limitations associated with conventional separation methods. The properites and performances of the AEMs were optimized by brominating poly(2,6-dimethyl-1,4-phenylene oxide) (PPO) polymers and the subsequent quaternization using tertiary amines of varying chain lengths to form quaternary ammonium bases, promoting their ion association with $[PdCl_4]^{2-}$. The AEM matrix optimization also involved adjusting polymer concentration, which affects the charge density, hydrophilicity, polymer network density, and microstructure of the membrane, thereby influencing the palladium recovery efficiency. A remarkable $[PdCl_4]^{2-}$ recovery rate of exceeding 90 % was achieved using the tailored AEMs after a 4-hour electrodialysis process.

1. Introduction

Palladium, known for its exceptional resistivity and stability against corrosion and oxidation, as well as its electrical properties, is a noble and precious metal extensively utilized in various industries, including automotive, medical, jewelry, catalytic, and electronics [1,2]. The wide range of applications for palladium has led to a continuous increase in demand. However, palladium naturally occurs in limited quantities in ores, and the combination of high demand and scarce reserves has raised concerns about the sustainability of its use in these applications [3]. Therefore, there has been a shift in focus towards the recycling and reclamation of industrial sources containing palladium, aiming to address the challenges related to sustainability and the depletion of natural sources.

Typically, the acidic effluents generated from industrial processes or materials, such as electronic devices, used catalysts, or electrode assemblies, contain palladium in varying amounts and complex forms [4,5]. As a result, the recovery of palladium from such sources has received significant attention. Several technologies have been successfully employed to recover palladium, including adsorption [6], extraction [2], and precipitation [7]. However, these separation methods are chemically intensive, have insufficient recovery rates, require regeneration steps, and result in a significant loss of palladium as residuals [3,8]. Moreover, it is undeniable that recovering them in trace amounts poses technological challenges.

Recently, membrane-based technologies have received significant attention for recovering target metal species. Specifically, liquid membranes, such as polymer inclusion membranes, supported liquid membranes, and hollow fiber supported liquid membranes, including mobile ionic liquid carriers, have found application in palladium recovery [4,9–14]. Several studies have investigated the palladium recovery in the form of anionic chlorocomplex, $[PdCl_4]^{2-}$. In this approach, the transportation of $[PdCl_4]^{2-}$ across the liquid membranes is facilitated by mobile carriers. Despite the remarkable recovery rates achieved through these membranes, they face significant challenges, including the use of toxic organic extractants for subsequent re-extraction of the metals, slow mass transport rate, the long-term stability, leakage of carrier molecules, loss of the solvent phase, swelling of the support swelling, chemical

* Corresponding author.
E-mail address: liyuan.deng@ntnu.no (L. Deng).

https://doi.org/10.1016/j.cej.2024.151037
Received 21 December 2023; Received in revised form 2 April 2024; Accepted 4 April 2024
Available online 6 April 2024

degradation, and saturation of the organic phase [15]. Consequently, there is a growing demand for efficient separation methods capable of recovering palladium species from solutions without encountering the reported obstacles.

Electrodialysis has emerged as a promising method for separating various types of metal species by leveraging an electric field to facilitate the transport of metal ions [16–18]. Compared to conventional techniques, electrodialysis offers notable advantages, including high recovery or removal rates for targeted species, even from diluted sources, while minimizing the use of harsh chemicals, avoiding phase changes, and reducing waste generation [19,20]. As a result, electrodialysis can efficiently purify valuable species with reduced environmental impact [21,22]. Given the significant benefits, liquid membranes have been employed in electrodialysis to treat effluent based on $[PdCl_4]^{2-}$ achieving the separation of $[PdCl_4]^{2-}$ from transition metals or platinum with a relatively high transport rate thanks to the aid of applied current, solidifying the significance of electrodialysis as a promising technology [23,24]. However, the concerns associated with the nature of liquid membranes mentioned above persist, regardless of the separation process.

Considering the importance of palladium recovery and the aforementioned limitations in traditional palladium recovery technologies, using anion exchange membranes (AEMs) in electrodialysis presents a promising strategy. AEMs are polymer films incorporating fixed positively charged groups within their matrix [25]. Hence, by exploring the potential of AEMs for palladium recovery in electrodialysis, it is possible to overcome the limitations associated with liquid membranes. So far, AEMs are used in electrolytic cells for various applications, such as the removal of harmful ions (e.g., halide anions) from hydrometallurgical streams, groundwater purification, and seawater desalination [26–28]. Controlling membrane compactness and charge density play a pivotal role in achieving intended separation [29–31]. Furthermore, AEMs play a crucial role in fuel cells by facilitating the conduction of hydroxyl ions for sustainable energy generation [32]. However, to the best of the authors' knowledge, the application of AEMs in solutions containing palladium species has not been studied, highlighting the need for immediate attention and further investigation in this area. Moreover, the application of conventional electrodialysis for precious metal recovery remains quite limited.

This study aims to design and tailor AEMs in electrodialysis for efficient and cost-effective recovery of $[PdCl_4]^{2-}$ from an industrial hydrochloric acid-based solution with a concentration of 1000 mg·L^{-1}, comprising metal residuals in trace amounts. AEMs, as an unexplored method for recovering $[PdCl_4]^{2-}$, have been developed with quaternary ammonium fixed groups from brominated poly(2,6-dimethyl-1,4-phenylene oxide) (BPPO) polymers, potentially overcoming limitations associated with previously mentioned methods in the literature. PPO is a promising choice for synthesizing AEMs due to its chemical and thermal stability, rendering it resistant to degradation in diverse electrolytes, acidic solutions, and varying temperatures. Furthermore, PPO possesses activated aromatic rings and allylic portions, enabling flexible functionalization through bromination and easy conversion into ammonium groups via quaternization. The optimization of the AEM matrix involved adjusting factors such as tertiary amines with varying alkyl spacer and polymer concentration to enhance $[PdCl_4]^{2-}$ transport through the membranes, influencing ion exchange capacity (IEC), hydrophilicity, and polymer network density. The resulting membranes were characterized through chemical structure analysis, morphological characteristics, physicochemical tests, and electrochemical evaluation. The study examined the influence of different membrane microstructures on the recovery rate of $[PdCl_4]^{2-}$ using the developed AEMs in electrodialysis. The electroosmotic water transfer (EWT) and conductivity through AEMs were also investigated, as it critically affected the rate of $[PdCl_4]^{2-}$ transport. The concentration of chloride ions (Cl^-) and solution pH were determined to investigate their effect on the $[PdCl_4]^{2-}$ transport rate as well as the complex forms of palladium species in the treated solutions, which were confirmed with UV analysis. This study highlights the pivotal importance of membrane material design to enhance precious metal ion conductivity while reducing water transport. The aim is to maximize resource recovery and minimize energy losses associated with industrial electrolyte solutions, suggesting significant potential of membrane technology in the recovery of noble and precious metals.

2. Materials and methods

2.1. Materials

PPO (the number average molecular weight M_n is 20,000 g·mol^{-1} and the number average molecular weight M_w is 30,000 g·mol^{-1}), N-bromosuccinimide (NBS, 99 %), 2,2′-Azobisisobutyronitrile (AIBN, 98 %), chloroform (99.5 %), chlorobenzene (99.5 %), ethanol (96 % and 100 %), trimethylamine (TMA, a 45 wt% aqueous solution), dimethylhexylamine (DMHA, 98 %), N-methyl-2-pyrrolidone (NMP, 99.5 %), deuterated chloroform ($CDCl_3$, 99 %), sodium chloride (NaCl), and sodium sulfate Na_2SO_4 were used as received from Aldrich, Germany. An industrial solution with a matrix composed of hydrochloric acid, palladium, and other metal residual with a pH below 1 was kindly provided by K.A. Rasmussen AS (Norway), which was used to assess the recovery performance of $[PdCl_4]^{2-}$. The composition of the industrial solution is tabulated in Table 1. PC SK end-CEMs (PCCell GmbH, Germany) were utilized in the electrodialysis tests. Silver nitrate ($AgNO_3$, 99 %, Aldrich) was used to determine Cl^- concentrations.

2.2. Bromination of PPO

PPO was brominated following the method described in our previous study [20]. Initially, 6 g (50 mmol) of PPO was dissolved in 100 mL of chlorobenzene in a flask equipped with a water-cooling condenser. Once the PPO was completely dissolved, 4.45 g (25 mmol) of NBS and 0.246 g of AIBN were added to initiate the bromination reaction. The reaction temperature was set at 135 °C to specifically target the bromination reaction on the benzyl positions, which are the sole sites responsible for anion exchange groups within the polymer network [20]. The reaction was conducted for 3 h in an oil bath while purging with argon. Following the reaction, the mixture was precipitated in 1000 mL of ethanol, filtered, and left to dry overnight. For further purification, 70 mL of chloroform was used to dissolve the resulting polymers. Subsequently, the polymers were precipitated again and washed with pure ethanol at 40 °C for 1 h to remove any residual solvent. Finally, the polymers were dried in a vacuum oven at 80 °C for 24 h.

2.3. Preparation of AEMs

A total of 1.5 g of BPPO was dissolved in NMP at different concentrations of 10 %, 15 %, and 20 % (w/w). The quaternization reaction was initiated by adding TMA or DMHA in a mole ratio of 2:1 to the brominated portion of the polymer. The reaction mixture was maintained at room temperature for 48 h. Subsequently, the reaction mixture was poured onto a glass plate and cast to a thickness of 700 μm. The cast solution was then placed in an oven at 60 °C under a vacuum for 24 h to evaporate the solvent. The resulting films were soaked in deionized water to facilitate their removal from the glass plate. The AEMs were named AEM-x-y, where x represents the BPPO amount in the reaction mixture as a weight percentage, and y indicates the tertiary amine used. The preparation route of AEMs is illustrated in Scheme 1, and the

Table 1
The composition of the industrial solution assessed.

Palladium (mg·L^{-1})	Platinum (mg·L^{-1})	Rhodium (mg·L^{-1})	Iron (mg·L^{-1})
~ 1000	< 20	< 5	< 10

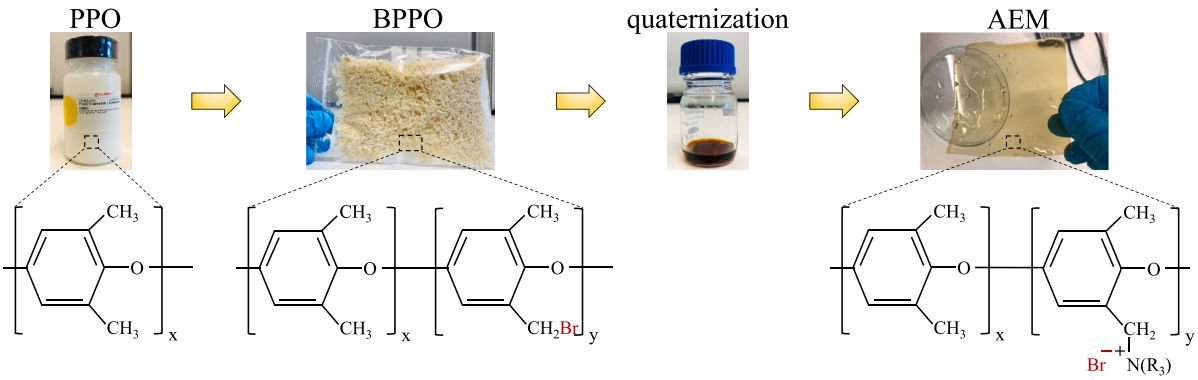

Scheme 1. The synthesis route of an AEM, including bromination of PPO and the quaternization of BPPO with tertiary amines.

composition of the different membrane feeds is provided in Table 2.

2.4. Characterization and methods

2.4.1. Chemical structure of the polymers and AEMs

The chemical structures of both the pristine and brominated polymers, along with the resulting AEMs, were analyzed using ^{1}H nuclear magnetic resonance (^{1}H NMR) on a Bruker Avance 600 Neo spectrometer and Fourier transform infrared spectroscopy (FT-IR) spectra. Deuterated $CDCl_3$ and DMSO-d_6 solvents were used to dissolve the polymers and membrane samples, respectively, and the ^{1}H NMR analysis was conducted at 600 MHz. The bromination degree at the benzyl position was determined by calculating the area under the respective peaks using Eq. (1) [33]:

$$\text{Bromination degree} = \frac{\text{Area peak at } 4.3}{\text{Area peak at } (6.4-7.0) + 2\cdot\text{Area peak at } (6.0-6.4)} \quad (1)$$

To further confirm the quaternization reaction, both the polymer and membrane samples were analyzed using FT-IR spectra. The FT-IR analysis was conducted using an iS50 FT-IR spectrometer from Thermo Scientific.

2.4.2. Morphological analysis

The surface and cross-section topography of the membranes were characterized by a scanning electron microscope (SEM, Zeiss SUPRA 55-VP) with a field emission electron gun. The SEM samples were cut into small pieces and dried at 50 °C before the analysis. Then, it was mounted in a sample holder and coated with a thin gold layer by a sputter coater (Quorum, Q150R ES) to make the samples electronically conductive.

2.4.3. Physicochemical properties of the AEMs

Small pieces of membrane samples were first dried in an oven at 60 °C and weighed. Then, the membrane samples were immersed in 1.0 M NaCl aqueous solution for 24 h to replace the bromide ions in the membrane with Cl^- from the solution. Afterward, the samples were rinsed with deionized water and soaked in 0.5 M Na_2SO_4 aqueous solution for another 24 h to exchange Cl^- with sulfate ions. The exchange solution containing Cl^- was titrated with 0.1 M $AgNO_3$. A potentiometric titration (Mettler Toledo, Easy Cl) was used to determine the Cl^- concentration. The following Eq. (2) was used to calculate the IEC values of the membranes [34]:

$$\text{IEC}\left(\frac{\text{mmol}}{\text{g}}\right) = \frac{V_{Na_2SO_4}\cdot C_{Cl^-}}{W_{dry}} \quad (2)$$

where $V_{Na_2SO_4}$ is the volume of Na_2SO_4 (L), C_{Cl^-} is the concentration of Cl^- (M), and W_{dry} is the dry weight of membrane samples (g).

The water uptake and swelling ratio of the membranes were determined by measuring the weight and dimensional changes between the dry and wet membrane samples. The membrane samples were cut into 2 cm x 4 cm sizes and dried in an oven at 60 °C for 24 h. The weight and length of the dried AEM samples were then measured. The dried membrane samples were subsequently soaked in deionized water for 24 h, and the weight and dimensions of the wet membrane samples were measured immediately after removing excess surface water. The water uptake and swelling ratio values of the membrane samples were calculated using Eqs. (3) and (4) [34]:

$$\text{Water uptake}\,(\%) = \frac{(W_{wet} - W_{dry})}{W_{dry}}\cdot 100 \quad (3)$$

$$\text{Swelling ratio}\,(\%) = \frac{(l_{wet} - l_{dry})}{l_{dry}}\cdot 100 \quad (4)$$

where W_{wet} and W_{dry} represent the mass of the wet and dry membrane samples, respectively, while l_{wet} and l_{dry} are the lengths of the wet and dry membrane samples, respectively.

The membrane fixed charge concentration (FCC) was calculated using Eq. (5), using the IEC and water uptake values [35]:

$$\text{FCC}\left(\frac{\text{mol}}{\text{L}}\right) = \frac{\text{IEC}}{\text{water uptake}}\cdot \rho_w \quad (5)$$

where ρ_w is the density water.

2.4.4. Water contact angle

The surface hydrophilicity of the AEM samples was evaluated by measuring the water contact angle using an optical tensiometer (T330, Biolin Scientific). The dried membrane samples were securely attached to a glass plate prior to the measurement. Four measurements were conducted for each membrane sample, with 4 μl of deionized water droplets used in each measurement.

2.4.5. Electroosmotic water transfer

The Micro BED System was utilized to measure the EWT of the AEMs. A detailed schematic representation of EWT measurement is presented in our previous work [20]. This system consists of a coulomb counting device, applying a charge package of 120 A·s for a given volume. Throughout the operation, a current of 0.3 A was applied. The diluate

Table 2
Synthesized AEMs with different polymer concentrations and tertiary amine types.

Polymer backbone	BPPO content (weight %)	Tertiary amine	AEM after quaternization	Thickness (μm)
BPPO	10	TMA	AEM-10-TMA	64.8 ± 1.2
	15	TMA	AEM-15-TMA	92.5 ± 3.5
	20	TMA	AEM-20-TMA	154.0 ± 1.0
	15	DMHA	AEM-15-DMHA	90.0 ± 3.5

chamber was circulated with a 1 M NaCl solution, while the electrode chamber was with a rinse solution of 0.25 M Na_2SO_4. The open chamber served as the concentrate chamber and was filled with a 1 M NaCl solution without circulation. The AEM under investigation was positioned between the end-CEM and the hydrophobic CEM (PC S 100, PCCell GmbH). The purpose of using end-CEMs and hydrophobic CEM was to minimize interference from the electrolyte solutions and control water transport, respectively. By applying a current, a specific quantity of water was transferred through the AEM from the diluate chamber into the concentrate chamber. The increase in volume in the concentrate chamber was measured using a pipette. The EWT value was determined using Eq. (6):

$$\mathrm{EWT}\left(\frac{\mathrm{mol\,H_2O}}{\mathrm{mol\,e^-}}\right) = \frac{\mathrm{dn}}{\mathrm{Q{\cdot}F^{-1}}} = \mathrm{d}\left(\frac{\rho{\cdot}V}{M_w}\right).\frac{F}{I{\cdot}dt} \tag{6}$$

where n, V, ρ, and M_w represent mole, volume (mL), density ($g \cdot mL^{-1}$), and molecular weight ($g \cdot mol^{-1}$) of water, respectively. Q denotes the amount of charge transported (Coulomb), F corresponds to the Faraday constant (96,485.3C · mol^{-1} e^-), I represents the applied current ($C \cdot s^{-1}$), and dt (s) is the time change.

2.4.6. Conductivity measurements

The conductivity of the membranes was measured using electrochemical impedance spectroscopy. All membranes were equilibrated in industrial solution for 24 h. Five samples of each type of membrane with diameters of 2 cm were cut. Impedance measurements were conducted using a Gamry Interface 5000E potentiostat, from an initial frequency of 100 Hz to 1 MHz, zero direct current, and an alternating current of 1 mA rms. The resistance of the stacks of 2 to 5 membranes were measured at a time in the system shown in Fig. 1. The measured resistance was plotted versus the thickness of the stack. A linear regression was constructed, and the slope of the resulting linear function was taken as the resistance purely from the membranes. The resistance per length of thickness of the membrane obtained from the impedance measurements was used to calculate the membrane conductivity by the following Eq. (7):

$$\kappa = \frac{l}{RA} \tag{7}$$

where R (Ω) is the resistance, l (cm) is the membrane thickness, A is the membrane area (cm^2), and κ is the membrane conductivity ($mS \cdot cm^{-1}$).

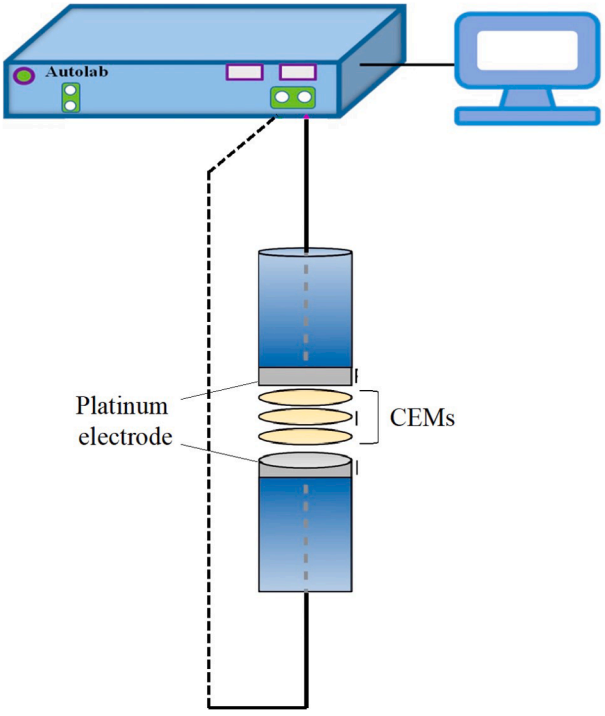

Fig. 1. Illustration of the cell used for electrochemical impedance measurements of the membranes. The cell was positioned in a vertical orientation, allowing the upper section to securely hold the membrane stack in place through the force of gravity.

2.4.7. Recovery measurements in electrodialysis

2.4.7.1. $[PdCl_4]^{2-}$ transport mechanism. The transport mechanism of $[PdCl_4]^{2-}$ is influenced by the specific type of ammonium groups present in the media, including quaternary, tertiary, or secondary ammonium ions. Each type of ammonium group plays a distinct role in the transport process. Secondary and tertiary ammonium groups function as weak base groups, while quaternary ammonium groups are strong base groups [36]. In the case of weak base groups, the interaction of $[PdCl_4]^{2-}$ occurs through a process known as chelation [37]. During chelation, covalent bonding takes place between the metal ions and the nitrogen atom of the functional group, facilitated by the donation of electrons [15,37]. This interaction forms a stable chelate complex. However, in order to complete the recovery process, subsequent elution of the $[PdCl_4]^{2-}$ from the base group is required [38].

On the other hand, quaternary ammonium groups are organic cations with a positive charge, while $[PdCl_4]^{2-}$ consists of a palladium ion coordinated with chloro ligands, which are negatively charged, promoting attractive forces between the two entities. Hence, when considering the ion association between $[PdCl_4]^{2-}$ and quaternary ammonium groups, it involves the formation of an ion pair through electrostatic interactions [36]. This ion pair formation can have significant implications for the transport of the $[PdCl_4]^{2-}$. The ion association enhances the solubility and mobility of the complex. Considering the aforementioned observations, incorporating the quaternary ammonium group as a pendant carrier in AEMs presents a promising strategy to achieve a more efficient exchange rate of $[PdCl_4]^{2-}$, allowing for the swift and effective transport of $[PdCl_4]^{2-}$ across the fixed charged groups without the need for subsequent elution steps. It is noteworthy that the interaction of $[PdCl_4]^{2-}$ has been reported in a specific order, namely quaternary > tertiary > secondary > primary [9]. This hierarchy implies that quaternary ammonium groups exhibit the highest affinity for $[PdCl_4]^{2-}$. The ion association and chelation mechanisms are identified in Eqs. (8) and (9), and visualized in Scheme 2a,b [37]:

$$[R_4N^+Cl^-]_{org} + [PdCl_4]^{2-}_{aq} \rightarrow [R_4N^+(PdCl_4)^-]_{org} + Cl^-_{aq} \tag{8}$$

$$[RNH_2^+Cl^-]_{org} + [PdCl_4]^{2-}_{aq} \rightarrow [RHN-(PdCl_3)^-]_{org} + H^+ + 2Cl^-_{aq} \tag{9}$$

In this study, the tertiary amines were incorporated into the backbone of BPPO to generate strong quaternary ammonium groups, aiming to facilitate the recovery of $[PdCl_4]^{2-}$.

2.4.7.2. Electrodialysis performance. Recovery measurements were conducted using a PCCell Micro BED System electrodialysis cell. The membrane stack consists of four chambers, including one diluate chamber, one concentrate chamber, and two electrode chambers. Custom-made AEMs were positioned in the middle of the cell, while commercial end-CEMs were placed at both ends of the stack to prevent interference from the rinse solutions in the feed chambers (Fig. 2). During the experiment, a 100 mL 0.25 M Na_2SO_4 rinse solution was circulated through the electrode chambers to generate a current of 0.5 A across the membranes, which had an effective area of 6 cm^2. The diluate and concentrate chambers were circulated with a 70 mL industrial solution. The feed was circulated at a flow rate of 120 $mL{\cdot}min^{-1}$. The electrodialysis measurement lasted for 240 min. Samples were collected at regular intervals from both the diluate and concentrate chambers to measure the concentration of $[PdCl_4]^{2-}$. The concentration of $[PdCl_4]^{2-}$ in the solution samples was analyzed using a microwave plasma-atomic

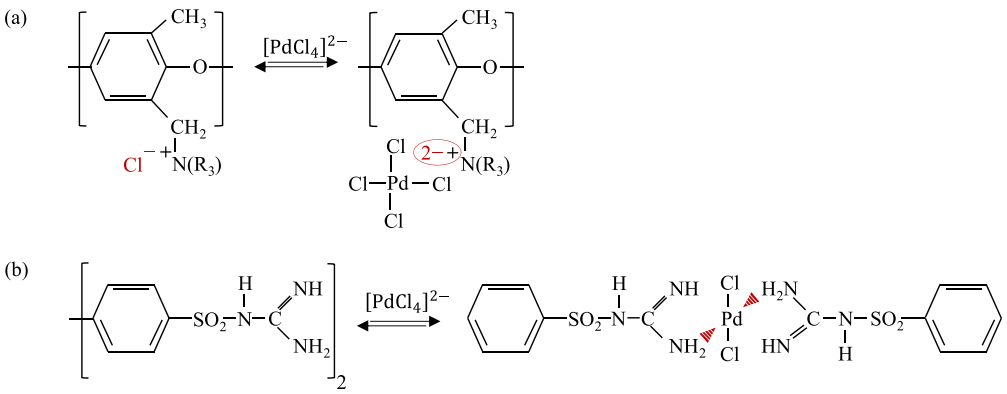

Scheme 2. Schematic of $[PdCl_4]^{2-}$ interaction with; (a) strong ammonium groups via ion association; (b) weak ammonium groups via chelation [37].

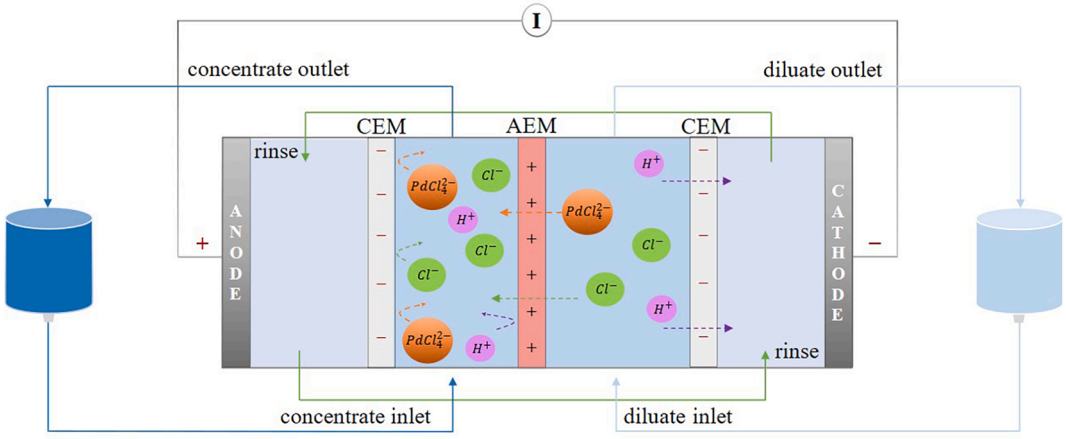

Fig. 2. Membrane stack assembly in an electrodialysis cell.

emission spectrometer (Agilent 4210), while Cl^- content in the solution samples was determined using Easy Cl (Mettler Toledo). To quantify the $[PdCl_4]^{2-}$ content in the membrane samples, a series of steps were followed. Firstly, the membranes were dissolved in aqua regia, and heat was applied to expedite the dissolution process. Any undissolved residue was carefully collected and placed in a crucible. To eliminate any organic components, the crucible containing the residue was subjected to high temperatures in an oven. Once the organic matter was completely burned off, the resulting ashes were dissolved in aqua regia. Finally, the solutions from both the initial leaching and the leaching of the ashes were combined and subjected to analysis using inductively coupled plasma optical emission spectroscopy, enabling the determination of the total palladium content present.

The transport mechanism of $[PdCl_4]^{2-}$ in electrodialysis involves the migration of charged palladium species under the influence of an electric field through the ion exchange process. During electrodialysis, an electric field is applied across the system, facilitating the release of $[PdCl_4]^{2-}$ into the concentrate compartment. Efficiencies of the resulting AEM system were defined in terms of the Eqs. (10) and (11) [9]:

$$\text{Removal efficieny}\,(\%) = \frac{C_{i,d} - C_{f,d}}{C_{i,d}} \cdot 100 \tag{10}$$

$$\text{Recovery efficieny}\,(\%) = \frac{C_{i,c} - C_{f,c}}{C_{i,c}} \cdot 100 \tag{11}$$

where $C_{i,d}$ ($mol \cdot L^{-1}$) and $C_{f,d}$ ($mol \cdot L^{-1}$) are the initial and final concentration of $[PdCl_4]^{2-}$ in the diluate, respectively, while $C_{i,f}$ and $C_{f,c}$ ($mol \cdot L^{-1}$) is the initial and final concentration of $[PdCl_4]^{2-}$ in the concentrate compartment. The molar flux of $[PdCl_4]^{2-}$ through the AEMs was determined using Eq. (12) [39]:

$$J_{[PdCl_4]^{2-}} = \frac{V \frac{dC_c}{dt}}{A} \tag{12}$$

where V (L) is the feed solution volume, dC_c ($mol \cdot L^{-1}$) is the concentration change of $[PdCl_4]^{2-}$, and A (m^2) is the active area of the membrane. The specific energy consumption (E_m) per mole of the transported $[PdCl_4]^{2-}$ was calculated from Eq. (13) [39]:

$$E_m = \frac{\int U_m \cdot I \cdot dt}{(C_{i,d} - C_{f,d}) \cdot V} \tag{13}$$

where U_m is the voltage drop across the cell, I is the applied current, and dt (s) is the time change.

The complex forms of palladium noble metal species in the solution samples from both diluate and concentrate compartments were predicted through pH and Cl^- measurements. These predictions were subsequently confirmed by MEDUSA software and UV measurements and presented in the Supporting Information (Figs. S1–S3). The pH of the initial and final solution samples was determined using a SevenDirectSD20 pH meter equipped with a high precision pH Sensor InLab Pro-ISM (Mettler Toledo). For the UV measurements, a Thermo Scientific UV–Visible spectrophotometer with a UVette cuvette of 10 mm path length was utilized. The absorbance data were processed using the Thermo Insight program. Spectra were recorded from 400 nm to 200 nm with a scan rate of 100 $nm \cdot min^{-1}$ and a resolution of 1 nm. Water was used as the reference.

3. Results and discussion

3.1. ^{1}H nuclear magnetic resonance and Fourier transform infrared spectroscopy

Fig. 3a displays the ^{1}H NMR spectra of PPO, BPPO, and AEMs. The successful verification of bromination in the benzyl group of the polymer was accomplished by observing new proton peaks at 4.3 ppm, which were not observed for PPO [33]. After the incorporation of tertiary amines (TMA or DMHA) into the polymer backbone, the ^{1}H NMR peak of the bromobenzylic proton at 4.3 ppm disappeared, and new benzylic proton peaks adjacent to the head group of quaternary ammonium group appeared at 3.1 ppm, providing evidence of quaternization, and more pronounced peaks can be observed in AEMs of increased polymer concentrations. This can be attributed to the greater abundance of brominated moieties due to high polymer concentration available for interaction with a higher quantity of amine groups, increasing the total fixed charge group in the membrane. Further increasing the polymer concentration to 20 % might not necessarily result in a proportionally increased quaternization of the benzylic brominated parts due to potential limitations in reactant access, yielding lower peak. It is worth noting that with the membrane featuring a quaternary ammonium group having a longer alkyl chain length (AEM-15-DMHA), a relatively lower quaternization peak was observed. DMHA likely impeded the ease of the quaternization reaction, thereby reducing the attachment of amines to the polymer backbone. Based on the distinct peaks observed in the ^{1}H NMR spectra, it can be concluded that quaternary ammonium groups were effectively grafted onto the BPPO backbones.

To confirm the occurrence of the quaternization reaction between the carbon atom in the methyl group adjacent to the bromine and the nitrogen atoms in the head groups of tertiary amines, the FT-IR spectra of PPO, BPPO, and AEMs were also subjected to analysis (Fig. 3b). The recorded spectral features at wavenumbers approximately 1185 cm^{-1}, 1305 cm^{-1}, 1469 cm^{-1}, and 1602 cm^{-1} were attributed to the

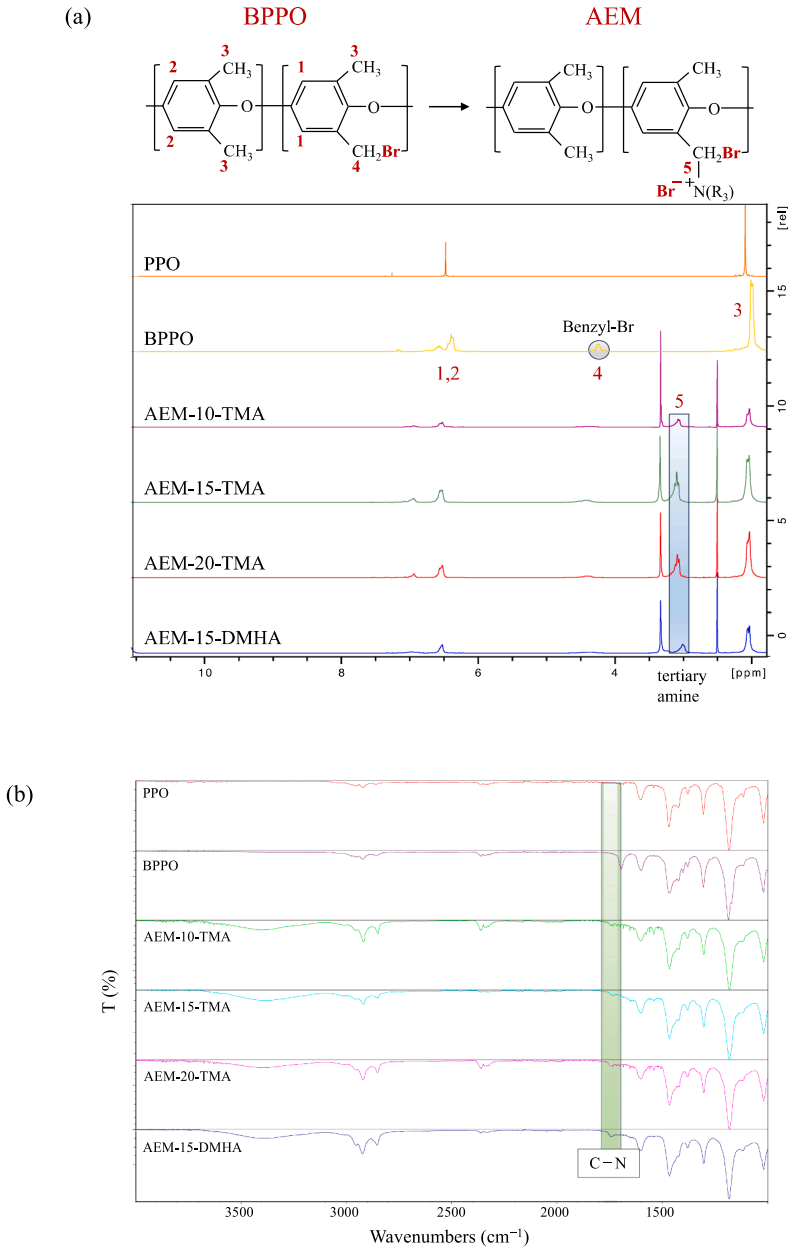

Fig. 3. The chemical structure of PPO, BPPO, and AEMs; (a) ^{1}H NMR spectra; (b) FT-IR spectra.

characteristic vibrations of the PPO polymer, whereas the band observed at approximately 1730 cm^{-1} was assigned to the vibrational mode of the C−N bond present in the quaternary ammonium groups [40,41]. Importantly, this distinctive band was absent in the spectra of both PPO and BPPO polymers, indicating the successful quaternization reaction. Additionally, a broad peak exhibiting a wavenumber of 3400 cm^{-1} emerged, corresponding to the O−H bond, signifying the presence of hydrophilic hydrated amine groups in AEMs, which was not observed for both PPO and BPPO polymers.

3.2. Morphology of AEMs

The AEMs were subjected to morphological analysis employing SEM technique. Fig. 4 provides visual presentation of surface topography and cross-section images of these membranes. The images reveal that the surfaces of all examined membranes exhibit a dense nature (Fig. 4a–d). However, a relatively loose and porous membrane bulk structure was observed, and the porosities and pore size vary depending on the polymer concentration in the cast solution and the type of tertiary amine used (i.e., TMA or DMHA). Therefore, the bulk matrix morphology of the AEMs was investigated using high resolution SEM images.

As can be seen in (Fig. 4e), at a low polymer concentration (10 %), the membrane bulk is nearly dense without visible pores. It is likely because that at a low polymer-to-solvent ratio, the solvent evaporation is fast, resulting in well packed polymer chains in the matrix and hence a more dense structure with negligible porosity [42]. Differently, when a polymer concentration higher than a threshhold value is employed, a skin layer may form first, impeding the evaporation of the solvent below the skin layer, such as in the cases of AEM-15-TMA and AEM-20-TMA. Due to the existing charged groups, microphase separation occurs, leading to formation of pores and channels within the polymer matrix, as shown in Fig. 4f and g. The porosity and pore size increased with the growing number of the charged groups in the cast solutions. This correlation is explained by the increased polymer concentration, requiring an increased amount of TMA to maintain a 2:1 mol ratio between TMA and the brominated part of the polymer. This effect was more pronounced when DMHA was introduced (Fig. 4h). The notably lower volatility and longer chains of DMHA led to a higher likelihood of phase separation and enhance formation of a more porous structure and larger size of ionic channels [43].

3.3. Ion exchange capacity, water uptake, swelling ratio, and fixed charge concentration

The IEC of the membrane is a metric that quantifies the number of fixed charges per unit mass of dry polymer in the membrane. This parameter provides valuable insights into the concentration of free charge within the membrane. The IEC is a critical property of the membrane that directly affects the transport rate of ions. Fig. 5a presents a range of IEC values observed for developed membranes. The IEC for AEM-15-TMA exhibited higher value, whereas AEMs synthesized with 10 % and 20 % polymer concentration displayed lower but fairly similar IEC values. Normally, an increase in polymer concentration should, in principle, yield a relatively consistent IEC per gram. This is attributable to the greater mass of both unbrominated and benzyl brominated segments as polymer content increases, thereby maintaining the number of fixed charges per unit mass of polymer at a consistent level despite a higher degree of quaternization. However, the differences in IEC values can be ascribed to either the lower polymer content, which may contain slightly less bromobenzylic moieties, or the higher polymer concentration leading to the formation of a denser network structure, limiting the access to the reactive sites. Notably, when TMA was replaced with DMHA for the same polymer concentration (15 %), the IEC remained lower due to the suppressed quaternization reaction.

Membranes with higher IEC values tend to exhibit more pronounced water uptake behaviors. This relationship clarifies the observed correspondence between the water uptake tendencies of the AEMs and their corresponding IEC magnitudes. Therefore, the AEM-15-TMA membrane displayed the highest water uptake among all the developed membranes. It is worth noting that AEM-15-DMHA exhibited the lowest water uptake value, a consequence attributed to the significant impact of a longer alkyl chain length, which contributes to a more hydrophobic environment within the membrane network [44].

Other important factors that influence ion transport across a dense membrane include membrane swelling degree and FCC, both of which are investigated for the developed AEMs (Fig. 5b). Ion sorption and mobility, as steps of ion transport through the membrane, are notably affected by the concentration of fixed charge groups and water content present within charged polymers. Therefore, the distribution and concentration of fixed charge groups, along with their associated water content within the AEMs, hold significant relevance in the context of ion transport. The swelling ratio of AEM-15-TMA was observed to be the highest, a phenomenon primarily attributable to its higher IEC and water uptake. The greater swelling characteristic of AEM-20-TMA compared to AEM-10-TMA can be attributed to its more porous structure. On the other hand, AEM-15-DMHA displayed the lowest degree of swelling, primarily due to the hydrophobic nature of the quaternary ammonium group. The results also revealed an inverse relationship between the swelling ratio and FCC. The stems from the fact that a membrane with high IEC leads to the increased swelling capacity due to the hydration of ion exchange groups, decreasing the FCC within the network. Notably, when DMHA was introduced in place of TMA, the FCC reached its maximum value despite comparable IECs. This outcome can be attributed to the relatively lower swelling ratio associated with

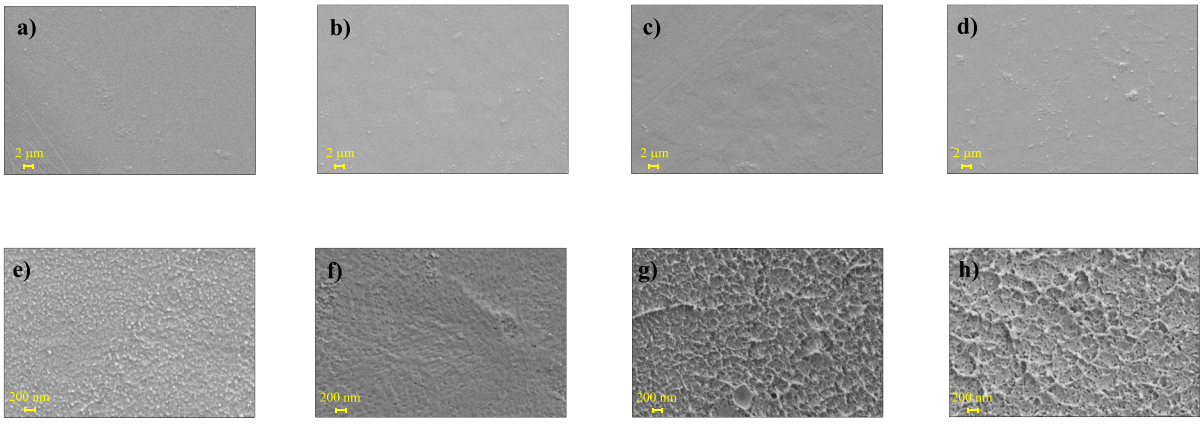

Fig. 4. SEM images of the AEMs; a,e) AEM-10-TMA; b,f) AEM-15-TMA; c,g) AEM-20-TMA; d,h) AEM-15-DMHA, and images a, b, c, and d are the mebrane surface; and e, f, g, and h are the high resolution SEM images of the membrane bulk matrices.

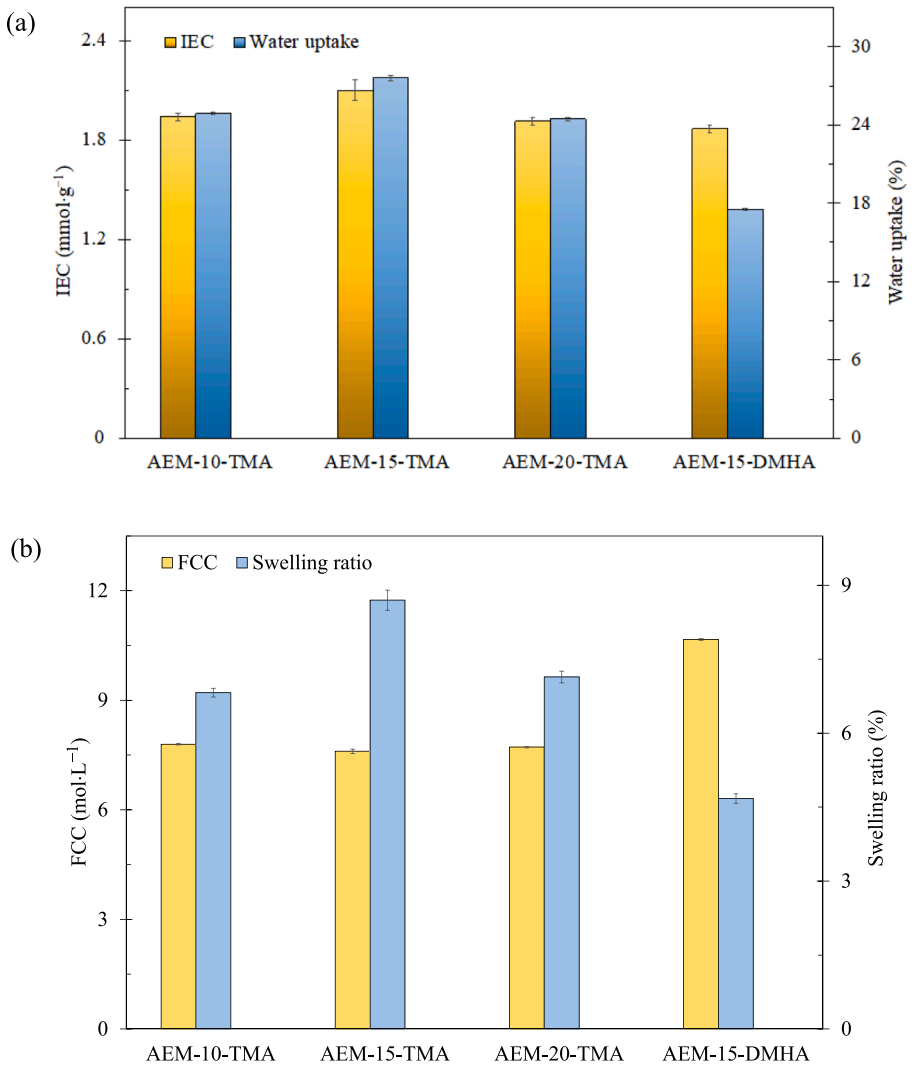

Fig. 5. (a) IEC and water uptake values; (b) swelling ratio and FCC values of the investigated AEMs.

DMHA.

3.4. Hydrophilicity of the membranes

Water contact angle measurements were conducted to assess the surface hydrophilicity of the AEMs (Fig. 6). AEM-15-TMA, with the

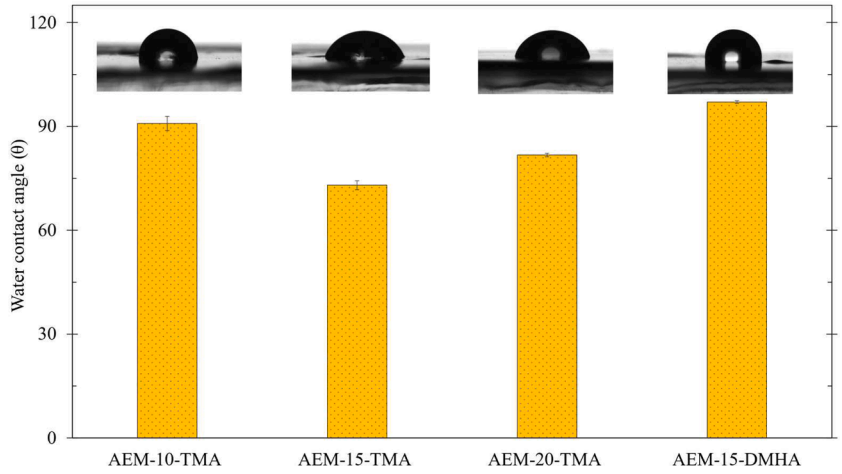

Fig. 6. Water contact angle values of the investigated AEMs.

highest IEC, was capable of absorbing the largest amounts of water among developed membranes, resulting in the lowest water contact angle value. On the other hand, the AEM-10-TMA membrane displayed a greater water contact angle than AEM-20-TMA despite both membranes having similar IEC values. This distinction can be attributed to the reduced count of total fixed charge groups in the membrane with lower polymer concentration. Additionally, maintaining a polymer concentration of 15 % and introducing hydrophobic side chains of DMHA into the polymer backbone led to a notably increased water contact angle. This structural modification hindered water retention by the polymer backbone, leading to a much higher hydrophobic surface.

3.5. Electroosmotic water transfer

The membrane's crucial role in excluding water transport is highlighted by its significant impact on the transportation of the target ion, directly influencing the recovery efficiency of the electrodialysis process. Consequently, the examination of the water transport properties of AEMs becomes imperative in analyzing the rate of $[PdCl_4]^{2-}$ transport. Under the influence of an electric current, the co-transport of water outweighs the osmotic flux, rendering the impact of water transport through osmosis negligible [45]. Therefore, the analysis primarily focuses on electroosmosis as the predominant factor to consider.

The transport of water varied among the investigated AEMs due to differences in their microstructures (Fig. 7). For instance, increasing polymer concentration from 10 % to 15 % increased water transfer due to elevated IEC and inherent hydrophilic characteristics [46]. However, membranes 20 % polymer content showed diminished water drag owing to their reduced IEC, lower swelling ratio and higher water contact angle compared to AEM-15-TMA. On the other hand, the introduction of hydrophobic alkyl chains within the AEM-15-DMHA membrane conferred a more hydrophobic structural framework, leading to a reduced capacity for water molecule absorption and improved anti-swelling properties, resulting in a substantial reduction in water transport. Furthermore, it is worth emphasizing that when Cl^- ions dissolve in water, they attract the positively charged hydrogen ends of water molecules, forming a stable structure around Cl^-, known as the hydration shell, which tends to release water molecules as they transport through hydrophobic membranes, thus less water co-transport occurrence with Cl^-. All of these factors suggest that membranes possessing a more pronounced hydrophobic structure significantly impede the migration of water.

3.6. Conductivity of the membranes

Fig. 8 presents data on the ionic conductivity of the membranes. The results show that the membrane conductivity, directly associated to the total number of ion exchange groups within the membrane, is greater in the AEMs made of a higher polymer concentration. As a result, AEM-15-TMA displayed an elevated overall charge density throughout the

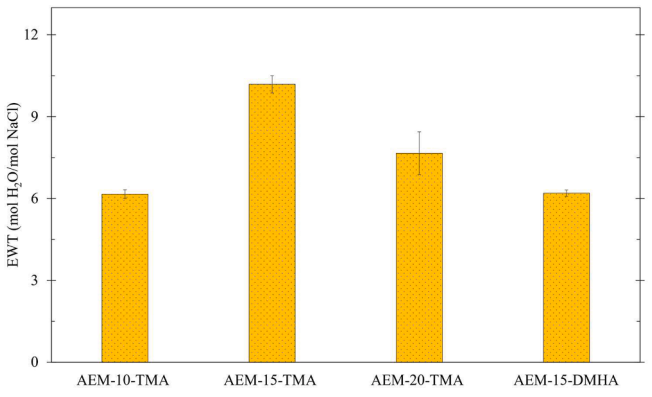

Fig. 7. EWT values of the investigated AEMs.

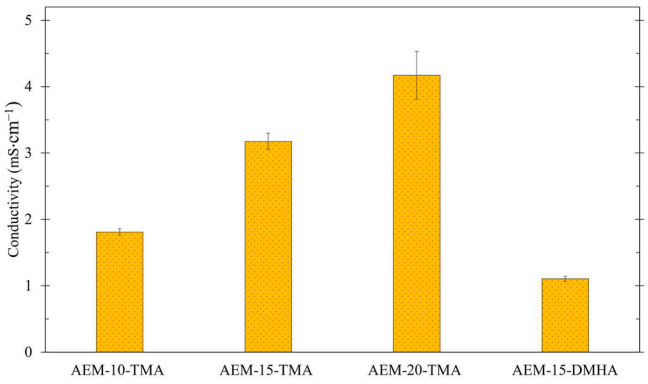

Fig. 8. Conductivity of the investigated AEMs.

membrane, rendering an enhanced conductivity when compared to membranes with lower polymer concentration (AEM-10-TMA). As the polymer concentration was further increased, a notable enhancement in conductivity was observed. This increase can be attributed to a more porous structure as confirmed by SEM in addition to an increased total charge within the membrane, which accelerated ion transfer.

Conversely, when the membrane contained a quaternary ammonium group with an extended alkyl chain, a substantial decrease in conductivity was observed. This can be attributed to the longer alkyl chains within the quaternary ammonium groups, which introduced steric hindrance and increased the separation between the charged amine group and its surrounding environment. This led to the formation of microdomains or amine group aggregation, disrupting the continuous pathways for ion transport within the membrane. Consequently, ions encountered longer, obstructed pathways, which reduced ion mobility. Moreover, longer alkyl chains resulted in a decreased IEC, leading to fewer available sites for ion exchange and transport, ultimately diminishing conductivity.

3.7. Recovery performances of the AEMs in electrodialysis

The transport ability of ions in electrodialysis is primarily governed by the characteristics of the employed membranes. In this study, we synthesized four AEMs with varying microstructures to explore their effects on the transport capabilities of $[PdCl_4]^{2-}$ and co-existing Cl^-, along with the recovery efficiency in an acidic feed solution, by conducting electrodialysis tests.

The $[PdCl_4]^{2-}$ is transported via electromigration from the bulk of the feed solution to the interface of the AEM, where they interact with fixed charge groups through ion association. Subsequently, $[PdCl_4]^{2-}$ ions transport into the concentrate compartment across the AEM. Fig. 9 illustrates the concentration profiles of $[PdCl_4]^{2-}$ in both the diluate and concentrate compartments, while Fig. 10 presents the removal and recovery efficiencies of the membranes, as well as the residual $[PdCl_4]^{2-}$ content in the membrane phase. Depending on the characteristics of the AEMs, distinct concentration profiles and $[PdCl_4]^{2-}$ transport rates were observed through the developed membranes (Fig. 10a). Moreover, detectable amounts of $[PdCl_4]^{2-}$ were observed in the AEMs after the electrodialysis tests. The residual $[PdCl_4]^{2-}$ content in the membrane phase varied depending on the characteristics of the AEMs (Fig. 10b).

The results indicate that the membrane fabricated with a polymer concentration of 10 % exhibited the most minimal change in $[PdCl_4]^{2-}$ concentration, implying the slowest transport of $[PdCl_4]^{2-}$ through the membrane. The similar color of the solutions from both diluate and concentrate compartments after the electrodialysis test also approves the inadequate transport of $[PdCl_4]^{2-}$ through AEM-10-TMA. Consequently, this particular membrane highlighted its limited ability to facilitate recovery of $[PdCl_4]^{2-}$ (20 $\pm$ 0.6 %). Notably, increasing the polymer concentration to 15 % and 20 % resulted in a substantial

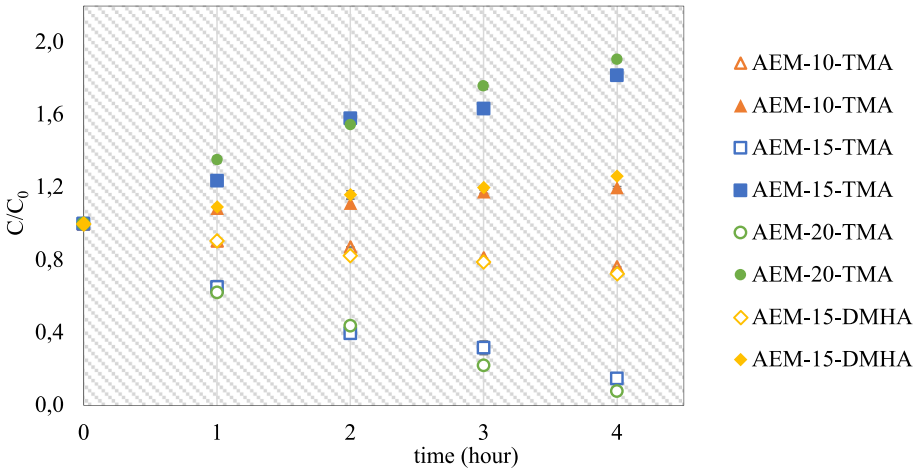

Fig. 9. Concentration profiles of $[PdCl_4]^{2-}$ in diluate and concentrate compartments across the developed AEMs during the electrodialysis tests. C_0 and C denote for the concentration of $[PdCl_4]^{2-}$ at time zero and t, respectively.

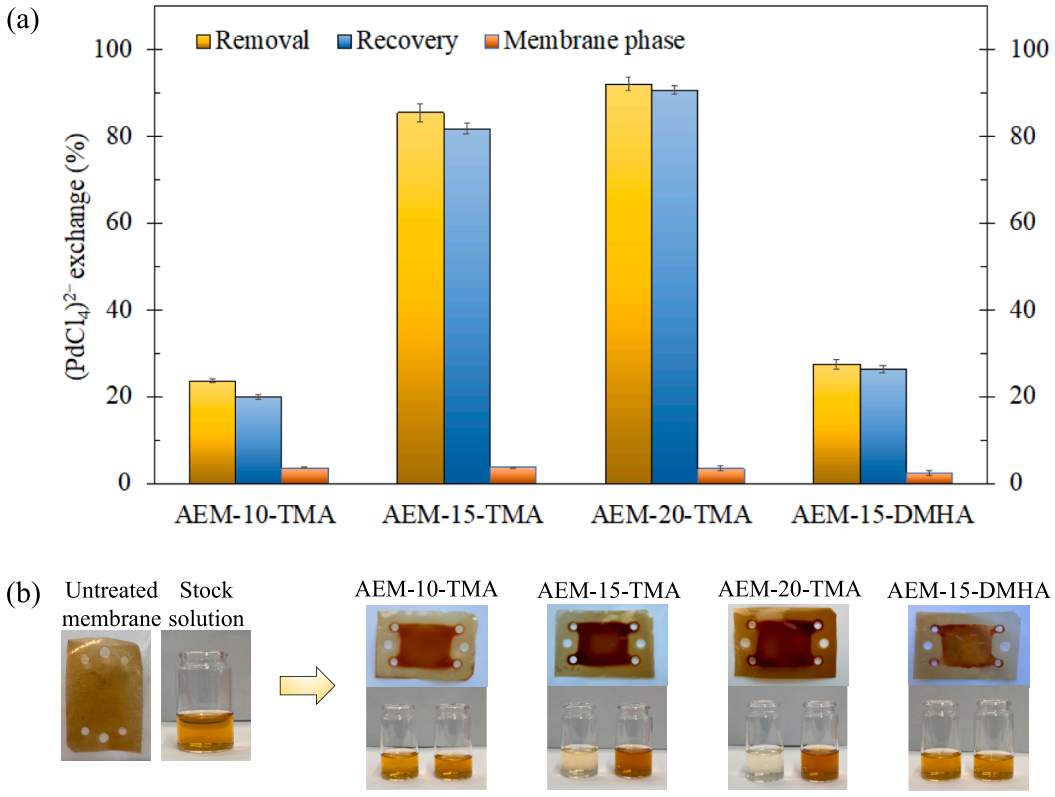

Fig. 10. (a) Percentage decrease in diluate compartment (removal), increase in the concentrate compartment (recovery), and residual in the membrane phase of $[PdCl_4]^{2-}$ after 4 h of electrodialysis. (b) The images depict AEMs and solution samples before and after electrodialysis. The untreated membrane and stock (feed) solutions refer to samples before electrodialysis. The right side of the arrow represents the membranes and the solutions, referring the diluate (left) and concentrate compartments (right), after 4 h of electrodialysis. The minimal color changes observed for the solutions obtained from the electrodialysis tests of AEM-10-TMA and AEM-15-DMHA indicated slow transport rate of $[PdCl_4]^{2-}$. In contrast, the solutions with significant color changes for AEM-15-TMA and AEM-20-TMA suggested a high transport rate of $[PdCl_4]^{2-}$ across them.

enhancement in recovery, with values ranging from 81.8 ± 1.2 % to 90.7 ± 1.0 %, respectively. Apparent color changes in solution samples have also supported the reported recoveries of $[PdCl_4]^{2-}$ upon completion of the electrodialysis process for the AEM-15-TMA and AEM-20-TMA membranes. It is also worth noting that AEM-15-TMA and AEM-20-TMA contained a higher amount of $[PdCl_4]^{2-}$, as confirmed by indicating the darker color observed for the membranes, supporting their high interaction with $[PdCl_4]^{2-}$. On the other hand, incorporating a hydrophobic chain length into the polymer network substantially reduced the recovery rate to 26.4 ± 0.8 % for AEM-15-DMHA, which contained the least amount of $[PdCl_4]^{2-}$ in its structure after electrodialysis.

The noticeable difference in $[PdCl_4]^{2-}$ recovery between AEM-10-TMA and AEM-15-TMA/AEM-20-TMA stems from disparities in both charge densities and membrane morphologies, which intricately influence the ionic conductivity, thereby exerting a significant impact on the

membranes' efficacy in recovery processes. AEM-10-TMA, characterized by its densely compacted structure and low matrix porosity, exhibited a low conductivity. This reduced conductivity directly correlates with a decelerated $[PdCl_4]^{2-}$ transport rate. On the other hand, the existing pores in membranes cast by increased polymer concentration elevate $[PdCl_4]^{2-}$ transport [47]. Another consequence of the higher conductivity is triggered by the higher charge density of the membranes, as observed in the cases of AEM-15-TMA and AEM-20-TMA (as substantiated by IEC and H-NMR analysis). Membranes with higher total charge and a more porous structure efficiently facilitate ion movement. Typically, such membranes demonstrate amplified ionic conductivity, contributing to the augmented $[PdCl_4]^{2-}$ recovery rate.

Another intriguing observation was the increase in $[PdCl_4]^{2-}$ upon increasing the polymer concentration of the membrane from 15 % to 20 %. A higher IEC value with a lower polymer content in AEM-15-TMA resulted in increased water content, leading to a lower wet membrane FCC (Fig. 5b) [48]. Moreover, a higher swelling ratio and water uptake increase the distance between fixed charge groups in a membrane, reducing the effectiveness of the Donnan potential for AEM-15-TMA compared to that of AEM-20-TMA [49,50]. The reduced potential weakens the attractive forces and slows down the transport of $[PdCl_4]^{2-}$, consequently lowering the recovery efficiency [51–54]. Furthermore, the electroosmotic water drag was lower through AEM-20-TMA compared to AEM-15-TMA, comparatively impeding the passage of water. This characteristic also enhances the concentration stage of the target $[PdCl_4]^{2-}$.

The investigation also included an analysis of the recovery efficiency of $[PdCl_4]^{2-}$ while mitigating water transport using a more hydrophobic membrane, achieved through the incorporation of quaternary ammonium groups with longer chain lengths as fixed charge groups (AEM-15-DMHA). Despite its highest FCC, a porous structure, and relatively low EWT, the presence of hydrophobic side-chains detrimentally affected the conductivity of the membrane. This impedance can be ascribed to the reduced density of exchangeable ions due to the inclusion of longer hydrophobic alkyl units, leading to weakened interactions with $[PdCl_4]^{2-}$, thereby hindering the transport rate of $[PdCl_4]^{2-}$. Nevertheless, it is essential to highlight that the performance of AEM-15-DMHA exceeded that of AEM-10-TMA. This observation potentially suggests that the membrane's porosity exerts a more pronounced influence on recovery performance, despite its lower conductivity, when compared to the denser yet more conductive AEM-10-TMA.

The recovery performance of $[PdCl_4]^{2-}$ by the best-performing AEM is compared with the existing literature, predominantly comprising different types of liquid membranes (Table 3). AEM-20-TMA demonstrates competitive $[PdCl_4]^{2-}$ recovery rates in electrodialysis, eliminating the need for elution process and the use of harsh organic phases. Importantly, this work introduces the effectiveness of AEMs for the first time within the author's knowledge, unveiling their immense potential in this particular field. Exploring different combinations of polymer materials to further optimize the microstructure of AEMs can enhance their performance in recovering $[PdCl_4]^{2-}$ within shorter electrodialysis process times. Moreover, unlike liquid membranes that can undergo carrier leaching and solvent evaporation, AEMs have huge potential to offer stable and long-lasting performance without requiring frequent replenishment, which can withstand diverse pH conditions, temperature variations, and chemical environments. Therefore, assessing the long-term stability of the AEM membranes in electrodialysis and implementing appropriate post-cleaning procedures are crucial steps when upscaling this process for precious metal recovery.

3.8. Transport rates and energy consumption

In electrodialysis, the interplay between the transport rates of ions and energy consumption is influenced by the magnitude of the applied voltage gradient. Fig. 11a depicts the fluxes of $[PdCl_4]^{2-}$ and Cl^-. The

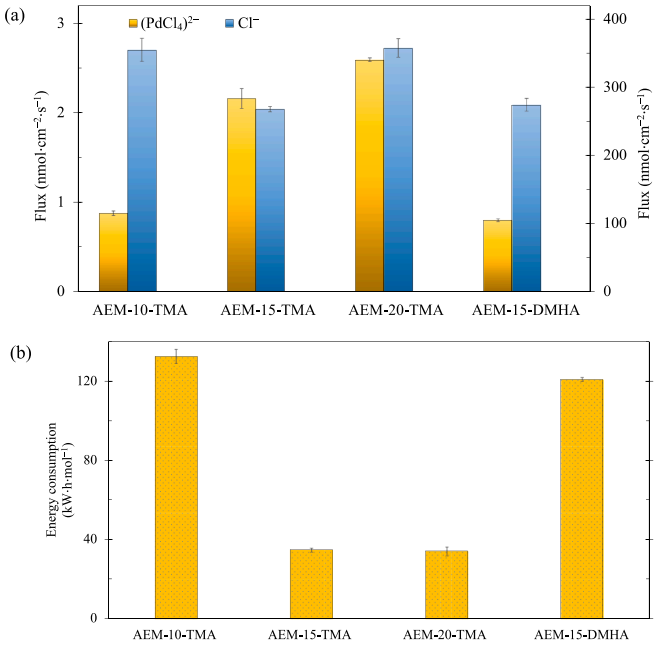

Fig. 11. (a) The fluxes of $[PdCl_4]^{2-}$ and Cl^- through investigated AEMs; (b) the energy consumption of the investigated AEMs per mole of $[PdCl_4]^{2-}$.

Table 3
Overview of $[PdCl_4]^{2-}$ recovery through membranes.

Membrane	Active group	Transport mechanism	Feed solution	Palladium concentration	Recovery	Ref
Supported liquid membrane	mobile carrier	facilitated transport of the Pd-carrier complex	diluted high level waste	1006 mg·L^{-1}	99.9 %	[11]
Hollow fiber supported liquid membrane	mobile carrier	facilitated transport of the Pd-carrier complex	spent automotive catalyst leachate	500 mg·L^{-1}	100 %	[12]
Hollow fiber supported liquid membrane	mobile carrier	facilitated transport of the Pd-carrier complex	industrial wastewater	100–400 mg·L^{-1}	91 %	[13]
Hollow fiber supported liquid membrane	mobile carrier	facilitated transport of the Pd-carrier complex	electronic wastewater	–	87.1 %	[9]
Polymer inclusion membrane	mobile carrier	facilitated transport of the Pd-carrier complex	model solution	1000 mg·L^{-1}	98 %	[10]
Polymer inclusion membrane	mobile carrier	facilitated transport of the Pd-carrier complex	model solution	0.001 M	87.2 %	[14]
Polymer inclusion membrane	mobile carrier	facilitated transport of the Pd-carrier complex	model solution	1000 mg·L^{-1}	95 %	[4]
AEM-20-TMA	fixed charge group	electromigration of $[PdCl_4]^{2-}$ in electrodialysis	industrial concentrated acid solution	1000 mg·L^{-1}	90.7 ± 1.0 %	This work

presented data demonstrates a significantly lower transport rate for $[PdCl_4]^{2-}$ compared to that of Cl^-. The differences in transport rates were more pronounced for membranes with superior hdyrophobicity (AEM-15-DMHA) and lower polymer concentration (AEM-10-TMA). The hydrophobic nature of AEM-15-DMHA allowed Cl^- to shed water molecules from its hydration shell due to its low energy of hydration, resulting in efficient transport through the membrane [55]. Moreover, AEM-10-TMA with denser structure impeded the transport of $[PdCl_4]^{2-}$, while facilitating the easier transport of Cl^-, owing to having higher diffusion coefficients and smaller size ($Cl^- > [PdCl_4]^{2-}$), thus resulting in substantial transport rate differences between Cl^- and $[PdCl_4]^{2-}$. On the contrary, the migration rate of $[PdCl_4]^{2-}$ was found significantly higher for AEM-15-TMA and AEM-20-TMA due to elevated total charge density and porosity within the membrane matrix, boosting ionic conductivity. Nevertheless, due to the concentration of Cl^- being approximately 400 times higher than that of $[PdCl_4]^{2-}$, with the former having a measured concentration of 1.5 M (Fig. S1), this difference significantly influences the charge transfer in favor of Cl^- during electrodialysis. Consequently, it leads to a notable difference in flux between $[PdCl_4]^{2-}$ and Cl^-.

The energy consumption of AEMs per mole of $[PdCl_4]^{2-}$ was calculated and presented in Fig. 11b. Notably, membranes with lower polymer concentration or longer hydrophobic alkyl units exhibited a higher energy consumption per mole of $[PdCl_4]^{2-}$, implying high resistance to the migration of $[PdCl_4]^{2-}$, thereby implying increased resistance to the migration of $[PdCl_4]^{2-}$. In contrast, AEMs with higher $[PdCl_4]^{2-}$ recovery (AEM-15-TMA and AEM-20-TMA) demonstrated notably lower energy consumption compared to membranes with lower recovery rates (AEM-10-TMA and AEM-15-DMHA). This observation suggests a correlation between energy consumption and the transport rate of $[PdCl_4]^{2-}$ across the membranes.

4. Conclusions

This study introduced a new approach utilizing AEMs in electrodialysis for recovering $[PdCl_4]^{2-}$ from an industrial solution, containing approximately 1000 $mg{\cdot}L^{-1}$ of palladium dissolved in hydrochloric acid with a pH below 1. The AEMs were custom-tailored through a two-step process involving bromination and quaternization of BPPO polymers with tertiary amines. Optimization of factors such as tertiary amines with varying alkyl spacer and polymer concentration substantially enhanced the recovery efficiency of $[PdCl_4]^{2-}$ by favorably influencing the membrane microstructure and fixed charge density.

The type of quaternary ammonium groups played a pivotal role in the ion association process. The inclusion of a quaternary ammonium group with a hydrophobic chain length in the polymer network substantially reduced the recovery rate due to the diminished density of exchangeable ions. Conversely, the incorporation of a hydrophilic quaternary ammonium group facilitated the transport rate of $[PdCl_4]^{2-}$. The polymer concentration in the casting solution significantly impacted membrane porosity. Increased polymer concentration notably improved the recovery efficiency of $[PdCl_4]^{2-}$ due to enhanced porosity and charge densities, thereby affecting membrane conductivity and the attractive forces between the positively charged pendant groups in the membrane and $[PdCl_4]^{2-}$. The residual $[PdCl_4]^{2-}$ content in the membrane phase varied based on AEM characteristics and remained relatively low, eliminating the need for subsequent elution steps. The transport rate of Cl^- was considerably higher compared to that of $[PdCl_4]^{2-}$, primarily due to high concentration difference between these ions.

As solid membranes, AEMs are easier to handle, shape, and integrate into systems. The unique properties of AEMs render them attractive candidates for use in electrodialysis, enabling the recovery of $[PdCl_4]^{2-}$ from secondary sources. This contribution aids in the development of sustainable and resource-efficient recovery methods. Further research and development, particularly in the field of hydrometallurgy, play a crucial role in unlocking the full potential of membrane-based technology in electrodialysis. This technology holds promise for recovering valuable metals from solution matrices, thereby addressing the challenges associated with their scarcity and the rising demand in various industries.

CRediT authorship contribution statement

Önder Tekinalp: Writing – review & editing, Writing – original draft, Visualization, Validation, Methodology, Investigation, Formal analysis, Data curation, Conceptualization. **Xueru Wang:** Writing – review & editing, Investigation. **Pauline Zimmermann:** Writing – review & editing, Methodology, Investigation. **Odne Stokke Burheim:** Writing – review & editing, Supervision, Funding acquisition, Conceptualization. **Liyuan Deng:** Writing – review & editing, Supervision, Resources, Project administration, Funding acquisition, Conceptualization.

Declaration of competing interest

The authors declare that they have no known competing financial interests or personal relationships that could have appeared to influence the work reported in this paper.

Data availability

Data will be made available on request.

Acknowledgments

The authors acknowledge the financial support from the Research Council of Norway through the PRICE project (No. 294543). The authors also thank colleagues from K.A. Rasmussen AS for technical assistance and the determination of palladium content in the membranes.

Appendix A. Supplementary data

Supplementary data to this article can be found online at https://doi.org/10.1016/j.cej.2024.151037.

References

[1] K. Fujiwara, A. Ramesh, T. Maki, H. Hasegawa, K. Ueda, Adsorption of platinum (IV), palladium (II) and gold (III) from aqueous solutions onto l-lysine modified crosslinked chitosan resin, J. Hazard. Mater. 146 (2007) 39–50, https://doi.org/10.1016/j.jhazmat.2006.11.049.

[2] T.H. Nguyen, C.H. Sonu, M.S. Lee, Separation of platinum(IV) and palladium(II) from concentrated hydrochloric acid solutions by mixtures of amines with neutral extractants, J. Ind. Eng. Chem. 32 (2015) 238–245, https://doi.org/10.1016/j.jiec.2015.08.022.

[3] A. Taghvaie Nakhjiri, H. Sanaeepur, A. Ebadi Amooghin, M.M.A. Shirazi, Recovery of precious metals from industrial wastewater towards resource recovery and environmental sustainability: A critical review, Desalination. 527 (2022) 115510, https://doi.org/10.1016/j.desal.2021.115510.

[4] A.T.N. Fajar, T. Hanada, M.L. Firmansyah, F. Kubota, M. Goto, Selective separation of platinum group metals via sequential transport through polymer inclusion membranes containing an ionic liquid carrier, ACS Sustain. Chem. Eng. 8 (2020) 11283–11291, https://doi.org/10.1021/acssuschemeng.0c03205.

[5] A.N. Nikoloski, K.L. Ang, D. Li, Recovery of platinum, palladium and rhodium from acidic chloride leach solution using ion exchange resins, Hydrometallurgy. 152 (2015) 20–32, https://doi.org/10.1016/j.hydromet.2014.12.006.

[6] R. Nagarjuna, S. Sharma, N. Rajesh, R. Ganesan, Effective adsorption of precious metal palladium over polyethyleneimine-functionalized alumina nanopowder and its reusability as a catalyst for energy and environmental applications, ACS Omega. 2 (2017) 4494–4504, https://doi.org/10.1021/acsomega.7b00431.

[7] F. Forte, S. Riaño, K. Binnemans, Dissolution of noble metals in highly concentrated acidic salt solutions, Chem. Commun. 56 (2020) 8230–8232, https://doi.org/10.1039/d0cc02298e.

[8] J.M. Arana Juve, F.M.S. Christensen, Y. Wang, Z. Wei, Electrodialysis for metal removal and recovery: A review, Chem. Eng. J. 435 (2022) 134857, https://doi.org/10.1016/j.cej.2022.134857.

[9] V. Mohdee, P. Ramakul, S. Phatanasri, U. Pancharoen, A numerical and experimental investigation on the selective separation of Pd (II) from wastewater

using Aliquat 336 via hollow fiber supported liquid membrane, J. Environ. Chem. Eng. 8 (2020) 104234, https://doi.org/10.1016/j.jece.2020.104234.
[10] A.T.N. Fajar, F. Kubota, M.L. Firmansyah, M. Goto, Separation of Pallaium(II) an Rhoium(III) using a polymer inclusion membrane containing a phosphonium-base ionic liqui carrier, Ind. Eng. Chem. Res. 58 (2019) 22334–22342, https://doi.org/10.1021/acs.iecr.9b05183.
[11] R. Ruhela, S. Panja, J.N. Sharma, B.S. Tomar, S.C. Tripathi, R.C. Hubli, A.K. Suri, Facilitated transport of Pd(II) through a supported liquid membrane (SLM) containing N, N, N', N'-tetra-(2-ethylhexyl) thiodiglycolamide T(2EH)TDGA: A novel carrier, J. Hazard. Mater. 229–230 (2012) 66–71, https://doi.org/10.1016/j.jhazmat.2012.05.064.
[12] C. Fontàs, V. Salvadó, M. Hidalgo, Selective enrichment of palladium from spent automotive catalysts by using a liquid membrane system, J. Memb. Sci. 223 (2003) 39–48, https://doi.org/10.1016/S0376-7388(03)00288-6.
[13] K. Wongkaew, U. Pancharoen, S. Phatanasri, N. Leepipatpiboon, A. W. Lothongkum, Effect of diluent polarity on membrane stability in the separation of trace Pd(II) from wastewater by HFSLM using LIX84-I, J. Ind. Eng. Chem. 21 (2015) 212–220, https://doi.org/10.1016/j.jiec.2014.02.027.
[14] B. Pospiech, Highly efficient facilitated membrane transport of palladium(II) ions from hydrochloric acid solutions through plasticizer membranes with cyanex 471x, Physicochem. Probl. Miner. Process. 51 (2015) 281–291, https://doi.org/10.5277/ppmp150125.
[15] H. Zheng, Y. Ding, Q. Wen, B. Liu, S. Zhang, Separation and purification of platinum group metals from aqueous solution: Recent developments and industrial applications, Resour. Conserv. Recycl. 167 (2021) 105417, https://doi.org/10.1016/j.resconrec.2021.105417.
[16] M. Sadrzadeh, A. Razmi, T. Mohammadi, Separation of different ions from wastewater at various operating conditions using electrodialysis, Sep. Purif. Technol. 54 (2007) 147–156, https://doi.org/10.1016/j.seppur.2006.08.023.
[17] C.V. Gherasim, J. Křivčík, P. Mikulášek, Investigation of batch electrodialysis process for removal of lead ions from aqueous solutions, Chem. Eng. J. 256 (2014) 324–334, https://doi.org/10.1016/j.cej.2014.06.094.
[18] M.F. San Román, I. Ortiz-Gándara, E. Bringas, R. Ibañez, I. Ortiz, Membrane selective recovery of HCl, zinc and iron from simulated mining effluents, Desalination. 440 (2018) 78–87, https://doi.org/10.1016/j.desal.2018.02.005.
[19] P. Zimmermann, Ö. Tekinalp, S.B.B. Solberg, Ø. Wilhelmsen, L. Deng, O. S. Burheim, Limiting current density as a selectivity factor in electrodialysis of multi-ionic mixtures, Desalination. 558 (2023), https://doi.org/10.1016/j.desal.2023.116613.
[20] Ö. Tekinalp, P. Zimmermann, O.S. Burheim, L. Deng, Designing monovalent selective anion exchange membranes for the simultaneous separation of chloride and fluoride from sulfate in an equimolar ternary mixture, J. Memb. Sci. 666 (2023), https://doi.org/10.1016/j.memsci.2022.121148.
[21] Ö. Tekinalp, P. Zimmermann, S. Holdcroft, O.S. Burheim, L. Deng, Cation exchange membranes and process optimizations in electrodialysis for selective metal separation : a review, Membranes (basel). 13 (2023) 566, https://doi.org/10.3390/membranes13060566.
[22] P. Zimmermann, Ö. Tekinalp, L. Deng, K. Forsberg, O.S.B. Wilhelmsen, Electrodialysis in hydrometallurgical processes, Miner. Met. Mater. Ser. (2020) 159–167, https://doi.org/10.1007/978-3-030-36758-9_15.
[23] T.Z. Sadyrbaeva, Extraction of Palladium(II) with liquid membranes based on Tri-n-Octylammonium and trialkylbenzylammonium chlorides under electrodialysis conditions, Russ. J. Appl. Chem. 94 (2021) 986–995, https://doi.org/10.1134/S107042722107017X.
[24] T.Z. Sadyrbaeva, Separation of palladium (II) and platinum (IV) by bulk liquid membranes during electrodilaysis, Sep. Sci. Technol. 41 (2020) 3213–3228.
[25] H. Strathmann, Electrodialysis, a mature technology with a multitude of new applications, Desalination. 264 (2010) 268–288, https://doi.org/10.1016/j.desal.2010.04.069.
[26] Y. Li, Z. Yang, K. Yang, J. Wei, Z. Li, C. Ma, X. Yang, T. Wang, G. Zeng, G. Yu, Z. Yu, C. Zhang, Removal of chloride from water and wastewater: Removal mechanisms and recent trends, Sci. Total Environ. 821 (2022) 153174, https://doi.org/10.1016/j.scitotenv.2022.153174.
[27] M. Grzegorzek, K. Majewska-Nowak, A.E. Ahmed, Removal of fluoride from multicomponent water solutions with the use of monovalent selective ion-exchange membranes, Sci. Total Environ. 722 (2020) 137681, https://doi.org/10.1016/j.scitotenv.2020.137681.
[28] H.F. Xiao, Q. Chen, H. Cheng, X.M. Li, W.M. Qin, B.S. Chen, D. Xiao, W.M. Zhang, Selective removal of halides from spent zinc sulfate electrolyte by diffusion dialysis, J. Memb. Sci. 537 (2017) 111–118, https://doi.org/10.1016/j.memsci.2017.05.009.
[29] W. Ji, B. Wu, Y. Zhu, M. Irfan, N. Ul Afsar, L. Ge, T., Xu, Self-organized nanostructured anion exchange membranes for acid recovery, Chem. Eng. J. 382 (2020) 122838, https://doi.org/10.1016/j.cej.2019.122838.
[30] Y.J. Lee, M.S. Cha, S.G. Oh, S. So, T.H. Kim, W.S. Ryoo, Y.T. Hong, J.Y. Lee, Reinforced anion exchange membrane based on thermal cross-linking method with outstanding cell performance for reverse electrodialysis, RSC Adv. 9 (2019) 27500–27509, https://doi.org/10.1039/c9ra04984c.
[31] M. Irfan, T. Xu, L. Ge, Y. Wang, T. Xu, Zwitterion structure membrane provides high monovalent/divalent cation electrodialysis selectivity: Investigating the effect of functional groups and operating parameters, J. Memb. Sci. 588 (2019) 117211, https://doi.org/10.1016/j.memsci.2019.117211.
[32] J.R. Varcoe, P. Atanassov, D.R. Dekel, A.M. Herring, M.A. Hickner, P.A. Kohl, A. R. Kucernak, W.E. Mustain, K. Nijmeijer, K. Scott, T. Xu, L. Zhuang, Anion-exchange membranes in electrochemical energy systems, Energy Environ. Sci. 7 (2014) 3135–3191, https://doi.org/10.1039/c4ee01303d.
[33] J. Parrondo, V. Ramani, Stability of Poly(2,6-dimethyl 1,4-phenylene)oxide-based anion exchange membrane separator and solubilized electrode binder in solid-state alkaline water electrolyzers, J. Electrochem. Soc. 161 (2014) F1015–F1020, https://doi.org/10.1149/2.0601410jes.
[34] L. Hao, J. Liao, Y. Liu, H. Ruan, A. Sotto, B. Van der Bruggen, J. Shen, Highly conductive anion exchange membranes with low water uptake and performance evaluation in electrodialysis, Sep. Purif. Technol. 211 (2019) 481–490, https://doi.org/10.1016/j.seppur.2018.09.042.
[35] B. Wei, J. Pan, J. Feng, C. Chen, S. Liao, Y. Yu, X. Li, Highly conductive and permselective anion exchange membranes for electrodialysis desalination with series-connected dications appending flexible hydrophobic tails, Desalination. 474 (2020) 114184, https://doi.org/10.1016/j.desal.2019.114184.
[36] R.A. Silva, K. Hawboldt, Y. Zhang, Application of resins with functional groups in the separation of metal ions/species–a review, Miner. Process. Extr. Metall. Rev. 39 (2018) 395–413, https://doi.org/10.1080/08827508.2018.1459619.
[37] J.C. Lee, H.J. Kurniawan, K.W. Hong, S.K. Chung, Separation of platinum, palladium and rhodium from aqueous solutions using ion exchange resin: A review, Sep. Purif. Technol. 246 (2020), https://doi.org/10.1016/j.seppur.2020.116896.
[38] R.S. Marinho, C.N. da Silva, J.C. Afonso, J.W.S.D. da Cunha, Recovery of platinum, tin and indium from spent catalysts in chloride medium using strong basic anion exchange resins, J. Hazard. Mater. 192 (2011) 1155–1160, https://doi.org/10.1016/j.jhazmat.2011.06.021.
[39] S. Abdu, M.C. Martí-Calatayud, J.E. Wong, M. García-Gabaldón, M. Wessling, Layer-by-layer modification of cation exchange membranes controls ion selectivity and water splitting, ACS Appl. Mater. Interfaces. 6 (2014) 1843–1854, https://doi.org/10.1021/am4048317.
[40] J. Pan, J. Ding, R. Tan, G. Chen, Y. Zhao, C. Gao, B. Van der Bruggen, J. Shen, Preparation of a monovalent selective anion exchange membrane through constructing a covalently crosslinked interface by electro-deposition of polyethyleneimine, J. Memb. Sci. 539 (2017) 263–272, https://doi.org/10.1016/j.memsci.2017.06.017.
[41] S.H. Roh, M.H. Lim, T. Sadhasivam, H.Y. Jung, Investigation on physico-chemical and electrochemical performance of poly(phenylene oxide)-based anion exchange membrane for vanadium redox flow battery systems, Electrochim. Acta. 325 (2019) 134944, https://doi.org/10.1016/j.electacta.2019.134944.
[42] E.N. Durmaz, M.I. Baig, J.D. Willott, W.M. De Vos, Polyelectrolyte complex membranes via salinity change induced aqueous phase separation, ACS Appl. Polym. Mater. 2 (2020) 2612–2621, https://doi.org/10.1021/acsapm.0c00255.
[43] M. Irfan, L. Ge, Y. Wang, Z. Yang, T. Xu, Hydrophobic side chains impart anion exchange membranes with high monovalent-divalent anion selectivity in electrodialysis, ACS Sustain. Chem. Eng. 7 (2019) 4429–4442, https://doi.org/10.1021/acssuschemeng.8b06426.
[44] X. Wang, X. Zhang, C. Wu, X. Han, C. Xu, Anion exchange membranes with excellent monovalent anion perm-selectivity for electrodialysis applications, Chem. Eng. Res. Des. 158 (2020) 24–32, https://doi.org/10.1016/j.cherd.2020.03.021.
[45] L. Han, S. Galier, H., Roux-de Balmann, Ion hydration number and electro-osmosis during electrodialysis of mixed salt solution, Desalination. 373 (2015) 38–46, https://doi.org/10.1016/j.desal.2015.06.023.
[46] W. Cheng, C. Liu, T. Tong, R. Epsztein, M. Sun, R. Verduzco, J. Ma, M. Elimelech, Selective removal of divalent cations by polyelectrolyte multilayer nanofiltration membrane: Role of polyelectrolyte charge, ion size, and ionic strength, J. Memb. Sci. 559 (2018) 98–106, https://doi.org/10.1016/j.memsci.2018.04.052.
[47] S. Mareev, A. Gorobchenko, D. Ivanov, D. Anokhin, V. Nikonenko, Ion and water transport in ion-exchange membranes for power generation systems: guidelines for modeling, Int. J. Mol. Sci. 24 (2023), https://doi.org/10.3390/ijms24010034.
[48] V.K. Shahi, A.P. Murugesh, B.S. Makwana, S.K. Thampy, R. Rangarajan, Comparative investigations on electrical conductance of ion-exchange membranes, Indian J. Chem. - Sect. A Inorganic, Phys. Theor. Anal. Chem. 39 (2000) 1264–1269.
[49] I. Stenina, D. Golubenko, V. Nikonenko, A. Yaroslavtsev, Selectivity of transport processes in ion-exchange membranes: Relationship with the structure and methods for its improvement, Int. J. Mol. Sci. 21 (2020) 1–33, https://doi.org/10.3390/ijms21155517.
[50] G.M. Geise, H.J. Cassady, D.R. Paul, B.E. Logan, M.A. Hickner, Specific ion effects on membrane potential and the permselectivity of ion exchange membranes, Phys. Chem. Chem. Phys. 16 (2014) 21673–21681, https://doi.org/10.1039/c4cp03076a.
[51] M.B. Kristensen, A. Bentien, M. Tedesco, J. Catalano, Counter-ion transport number and membrane potential in working membrane systems, J. Colloid Interface Sci. 504 (2017) 800–813, https://doi.org/10.1016/j.jcis.2017.06.010.
[52] M. Tedesco, H.V.M. Hamelers, P.M. Biesheuvel, Nernst-Planck transport theory for (reverse) electrodialysis: I. Effect of co-ion transport through the membranes, J. Memb. Sci. 510 (2016) 370–381, https://doi.org/10.1016/j.memsci.2016.03.012.
[53] G.M. Geise, M.A. Hickner, B.E. Logan, Ionic resistance and permselectivity tradeoffs in anion exchange membranes, ACS Appl. Mater. Interfaces. 5 (2013) 10294–10301, https://doi.org/10.1021/am403207w.
[54] M. Rodrigues, T. Sleutels, P. Kuntke, C.J.N. Buisman, H.V.M. Hamelers, Effects of current on the membrane and boundary layer selectivity in electrochemical systems designed for nutrient recovery, ACS Sustain. Chem. Eng. 10 (2022) 9411–9418, https://doi.org/10.1021/acssuschemeng.2c01764.
[55] R. Epsztein, E. Shaulsky, N. Dizge, D.M. Warsinger, M. Elimelech, Role of ionic charge density in donnan exclusion of monovalent anions by nanofiltration, Environ. Sci. Technol. 52 (2018) 4108–4116, https://doi.org/10.1021/acs.est.7b06400.